ELSEVIER

FEMS Microbiology Letters 220 (2003) 295–301

FEMS MICROBIOLOGY Letters

www.fems-microbiology.org

Analysis of metabolic and physiological responses to *gnd* knockout in *Escherichia coli* by using C-13 tracer experiment and enzyme activity measurement

Zhao Jiao [a], Tomoya Baba [b], Hirotada Mori [b], Kazuyuki Shimizu [a,c,*]

[a] *Metabolome Unit, Institute for Advanced Biosciences, Keio University, Yamagata 997-0017, Japan*

[b] *Genome Engineering Unit, Institute for Advanced Biosciences, Keio University, Yamagata 997-0017, Japan*

[c] *Department of Biochemical Engineering and Science, Kyushu Institute of Technology, Iizuka, Fukuoka 820-8502, Japan*

Received 11 November 2002; received in revised form 15 January 2003; accepted 14 February 2003

First published online 7 March 2003

Abstract

The physiological and metabolic responses to *gnd* knockout in *Escherichia coli* K-12 was quantitatively investigated by using the ^{13}C tracer experiment (GC-MS/NMR) together with the enzyme activity analysis. It was shown that the general response to the gene knockout was the local flux rerouting via Entner–Doudoroff pathway and the direction reversing via non-oxidative pentose phosphate pathway (PPP). The mutant was found to direct higher flux to phosphoglucose isomerase reaction as compared to the wild-type, but the respiratory metabolism was comparable in both strains. The anaplerotic pathway catalyzed by *malic enzyme* was identified in the mutant, which was accompanied with an up-regulation of phosphoenolpyruvate carboxylase and down-regulation of phosphoenolpyruvate carboxykinase. The presented results provide first evidence that compensatory mechanism existed in PPP and anaplerotic pathway in response to the *gnd* deletion.

Keywords: Gene deletion; Pentose phosphate pathway; ^{13}C tracer experiment; Enzyme activity; Metabolic response

1. Introduction

Precise understanding of metabolic and physiological responses to individual gene deletion can provide deeper insights into the control and regulation of the central metabolism of an organism. In the case of *Escherichia coli*, such studies have been primarily focused on the deletion of certain genes in the Embden–Meyerhof pathway (EMP) [1,2]. The pentose phosphate pathway (PPP), a major route of glucose utilization apart from EMP, has received less attention in regard to metabolic regulation. So far, no detailed information on the metabolic responses to PPP enzyme deletion is available except for certain phenotypic characterization [3,4]. Therefore, the conclusions on PPP were merely drawn based on qualitative interpretation of these physiological analysis. To reveal cause and effect relationships, however, it is important to further understand PPP in view of carbon flux distribution and enzyme expression.

Recent advances in isotopic tracer experiment enable a more comprehensive analysis of cellular metabolism by way of labeled cellular amino acids which are detectable by either mass spectrometry (MS) [5] or nuclear magnetic resonance (NMR) spectroscopy [6,7]. In the case of gene disruption mutants, however, an independent use of only one set of isotopic tracer data often could not fulfill the requirement of this complicated metabolic system, since either a rerouting of carbon fluxes or a reversing of primary direction might occur inside the mutants. To elucidate this complicated metabolic system, more information is therefore needed as compared with the study of its parent strain. The one possible solution is to combine 2D

* Corresponding author. Tel.: +81 (948) 29 7817; Fax: +81 (948) 29 7801.

E-mail address: shimi@bse.kyutech.ac.jp (K. Shimizu).

0378-1097/03/$22.00 © 2003 Published by Elsevier Science B.V. on behalf of the Federation of European Microbiological Societies.
doi:10.1016/S0378-1097(03)00133-2

NMR tracer data with mass isotopomer analysis. Such combination increases considerably the information obtained, but necessitates a more complicated algorithm to incorporate tracer data from different sources into the metabolic network model; the other useful method is to introduce in vitro enzyme activity analysis to the network identification, by which the alternative pathways due to gene disruption could be qualitatively identified and then the flux distribution analysis could be performed based on this identified network.

In the present study, we used complementary methods of ^{13}C tracer experiment (GC-MS and 2D NMR) together with in vitro enzyme activity measurement to quantitatively investigate the control and regulation of the PPP. We specifically targeted the 6-phosphogluconate dehydrogenase (6PGDH) deletion, as this enzyme (coded by *gnd* gene) plays a key role in the PPP due to its location at the link between oxidative PPP and non-oxidative PPP as well as its involvement in NADPH formation. The disruption is expected to cause flux rerouting and trigger the compensatory mechanism, from which the regulation of PPP could be quantitatively characterized and the metabolism in response to such variation could be clearly known. This could provide valuable information on the further gene engineering for the metabolic pathways.

2. Materials and methods

2.1. Strains and growth conditions

Two *E. coli* K-12 strains – wild-type BW25113 (*lacI*^{q} rrnB$_{T14}$ ΔlacZ$_{WJ16}$ *hsdR514* ΔaraBAD$_{AH33}$ Δ*rhaBAD*$_{LD78}$) and its *gnd* gene knock-out mutant (JWK 2011) – were used throughout this study. The mutant was obtained by one-step inactivation of chromosomal *gnd* gene using PCR primers [8] and was further confirmed by PCR strategy and in vitro enzyme activity analysis.

All batch and chemostat cultivations were performed with the same minimal medium prepared as described previously [9] with the exception for glucose concentration: 5 g l^{-1} for batch cultivation and 4 g l^{-1} for chemostat culture. Batch and chemostat cultures were conducted at 37°C in a 2-l reactor (Able Co., Japan) with pH controlled at 7.0. The airflow was maintained at 0.5 l min^{-1}, and the dissolved oxygen (DO) concentration was kept above 30% air saturation. The dilution rate for chemostat culture was 0.2 h^{-1}.

Labeling experiments were initiated after the chemostat culture reached a steady state, which was inferred from the stable O_2 and CO_2 concentrations in the off-gas and stable optical density in the effluent medium for at least twice as long as the residence time. The feed medium containing 4 g of unlabeled glucose per liter was then replaced by an identical medium containing the mixture of 0.4 g uniformly labeled glucose [U-^{13}C], 0.4 g first carbon labeled glucose [1-^{13}C] and 3.2 g of naturally labeled glucose per liter. Biomass samples for GC-MS/NMR analysis were taken after one residence time, and the labeling measurements were corrected for the remaining original (non-labeled) biomass that was still present at the end of the labeling experiment [10].

2.2. Analytical procedures

Cellular dry weight (CDW) was monitored by OD_{600} and calculated from previously determined OD-to-CDW correlations. Glucose was determined with commercial kits (Wako Co., Japan). Acetate concentration was determined by HPLC (Waters Co., Milford, MA, USA). Protein concentration was measured by the method of Lowry et al. [11]. Physiological parameters were calculated as described previously [12].

Preparation of crude cell-free extracts and analysis of key enzyme activities involved in the central metabolism were based on standard or modified enzymological methods [13]. Specific Entner–Doudoroff (ED)-pathway activity was determined from the combined *edd* and *eda* reactions [2].

Preparation of biomass hydrolysates and recording of GC-MS (Perkin Elmer) and 2D-NMR (Bruker) spectra were performed as described previously [9,14]. The program Turbomass Gold (Perkin Elmer) was used for peak assignment and MS data processing. Skewing effect of natural isotopes was corrected based on the algorithm proposed by Paul Lee [15]. In the case of the 2D-NMR spectra processing, the assignment of carbon signals was performed according to the previously described protocol [16] and the program WINNMR (Bruker) was used to quantify the relative contributions of singlet, doublet, and doublet of doublet signals to the overall multiplet patterns.

2.3. Mathematical modeling for flux calculation

The metabolic network considered is based on Neidhardt et al. [17] and Internet-accessible *EcoCyc* as well as the additional enzyme activity analysis. The flux calculation was accomplished by a full isotopomer model [18] together with a modified minimization model (Genetic algorithm plus Levenberg–Marquardt algorithm) as described previously [9]. The isotopomer model was used to simulate expected measurements as a function of a given set of intracellular fluxes. The best-fit intracellular fluxes can then be estimated by minimization of the deviation between experimental data and the simulated results using an iterative scheme within the minimization algorithm. A set of intracellular fluxes (including net fluxes and exchange fluxes) that gives the minimum deviation can be taken as the best estimate for the intracellular flux distribution. Matlab language (Math) was used to perform all these complicated calculations.

Table 1
Exponential growth parameters of aerobic *E. coli* batch cultures with glucose as the sole carbon source

Parameter	Wild-type BW25113	*gnd* knock-out mutant
μ_{max} (h^{-1})	0.62	0.60
Q_{glc} (mmol g^{-1} h^{-1})[a]	5.64	6.08
Q_{ace} (mmol g^{-1} h^{-1})[b]	1.24	2.00
Q_{CO2} (mmol g^{-1} h^{-1})[c]	4.19	4.15
Q_{O2} (mmol g^{-1} h^{-1})[d]	6.50	6.62
$Y_{X/S}$ (g g^{-1})[e]	0.61	0.54

Results represent the average of two different experiments.
[a]Specific glucose consumption rate.
[b]Specific acetate production rate.
[c]Specific CO_2 evolution rate.
[d]Specific O_2 consumption rate.
[e]Yield of biomass on glucose.

3. Results and discussion

3.1. Physiological response to 6PGDH deletion

To investigate the physiological effects of 6PGDH deletion, batch cultivation was used to determine the exponential growth parameters of the wild-type and the mutant (Table 1). It was found that although a single deficiency in *gnd* has little effect on the growth rate of *E. coli* on glucose, the two strains showed difference with respect to glucose consumption as well as acetate production rates, both of which were higher in the mutant. The specific oxygen consumption rate and CO_2 evolution rate varied little between two different cultures, indicating that there are only minor changes in respiratory metabolism. Although more glucose remained unutilized for the wild-type, the final cell concentration was almost the same in these two cultures. Accordingly, the apparent biomass yield ($Y_{X/S}$) was lower in the mutant in spite of very similar growth rates and respiratory activities. Hence, we conclude that the physiological consequences due to a *gnd* deletion are mainly manifested in reduced carbon utilization efficiency. The fact that the *gnd* deletion can potentially be compensated for by cellular compensatory mechanism allows us to further investigate the metabolic response in view of enzyme expression and carbon flux distribution.

3.2. Enzyme expression in response to 6PGDH deletion

To investigate the metabolic consequences of *6PGDH* deletion, key enzymes participating in the central metabolism were measured from cells under the condition of the mid-exponential growth phase (Table 2). It was shown that the levels of some key enzymatic activities varied greatly in these two strains. The significant effect caused by *gnd* deletion is the activation of Entner–Doudoroff (ED)-pathway and induction of the *malic* enzyme, which was accompanied by an up-regulation in phosphoenolpyruvate carboxylase (*ppc*) and down-regulation in phosphoenolpyruvate carboxykinase (*pckA*). Moreover, higher enzyme activity involved in the conversion of glucose-6-phosphate to fructose 6-phosphate (phosphoglucose isomerase) was found in the mutant, indicating that more carbon substrates were directed to EMP. This is supported by the decrease in the level of glucose-6-phosphate dehydrogenase. Interestingly, the non-oxidative PPP was still active, although the entrance via 6PGDH had been blocked. Apparently, the non-oxidative PPP must then proceed in an opposite direction from fructose-6-phosphate and glyceraldehyde-3-phosphate. Isocitrate dehydrogenase and malate dehydrogenase activities were comparable in extracts of both strains, which is consistent with the finding in the physiological analysis that there were only minor changes in respiratory metabolism when *gnd* was deleted.

Since in bacteria, glucose may take the route of catabolism via glucose ⇒ gluconate ⇒ gluconate-6-phosphate ⇒ ED (so-called GCD pathway) [19]. To check if the ED-pathway activity in the mutant was induced by GCD pathway, glucose dehydrogenase and gluconate kinase activity,

Table 2
Activities of key enzymes of *E. coli* BW25113 and its *gnd* mutant from exponential growth phase[a]

Pathway branch	Enzyme	Wild-type	*gnd* mutant
	glucose-6-phosphate dehydrogenase	354	248
Oxidative PPP	6PGDH	381	N.D.[b]
Non-oxidative PPP	transaldolase	909	393
	isocitrate dehydrogenase	1205	1229
TCA cycle	malate dehydrogenase	368	372
EMP	*P. isomerase*	1277	1675
ED-pathway	phosphogluconate dehydratase and KDPG-aldolase	N.D.	398
	malic enzymes	N.D.	70
Anaplerotic pathway	phosphoenolpyruvate carboxylase	406	497
Glucogenesis	phosphoenolpyruvate carboxykinase	39	N.D.

[a]Activities are given in nmol per min per mg protein except for the ED-pathway activity which was given as amount of pyruvate production nmol per 30 min per mg protein. Results represent the average of three different experiments.
[b]N.D.: Could not be detected by the employed enzyme activity analysis.

Table 3
Experimental determined (Exp) and calculated (Cal) fragment mass distribution of *N*-(tert-butyldimethylsilyl)-*N*-methyl-trifluoroacetamide-derivatized amino acids from wild-type and *gnd* mutant strains

Species			Wild-type BW25113			*gnd*$^-$ mutant		
Amino acids	fragment	origin	*m0*	*m1*	*m2*	*m0*	*m1*	*m2*
Val	$[M-57]^+$	Exp:	0.8230	0.0554	0.0645	0.8408	0.0511	0.0523
		Cal:	0.8188	0.0594	0.0642	0.8427	0.0493	0.0523
Ser	$[M-159]^+$	Exp:	0.9093	0.0278	0.0629	0.9107	0.0296	0.0597
		Cal:	0.9083	0.0287	0.0630	0.9117	0.0284	0.0598
Phe	$[M-159]^+$	Exp:	0.7842	0.0435	0.0983	0.7874	0.0458	0.0935
		Cal:	0.7805	0.0474	0.0977	0.7891	0.0440	0.0937
Glu	$[M-57]^+$	Exp:	0.7747	0.1025	0.0978	0.7830	0.0979	0.0964
		Cal:	0.7745	0.0992	0.1012	0.7872	0.0961	0.0949
Leu	$[M-159]^+$	Exp:	0.7640	0.1079	0.1004	0.7822	0.1039	0.0914
		Cal:	0.7653	0.1072	0.1003	0.7846	0.1018	0.0914
Ile	$[M-57]^+$	Exp:	0.7476	0.1196	0.0791	0.7470	0.1251	0.0827
		Cal:	0.7462	0.1205	0.0793	0.7518	0.1231	0.0812
Thr	$[M-57]^+$	Exp:	0.8106	0.1168	0.0350	0.8056	0.1226	0.0435
		Cal:	0.8102	0.1174	0.0351	0.8092	0.1202	0.0429
Ala	$[M-159]^+$	Exp:	0.9088	0.0281	0.0631	0.9154	0.0273	0.0573
		Cal:	0.9095	0.0277	0.0627	0.9178	0.0265	0.0557

The calculated values are from the estimated flux distribution given in Figs. 1 and 2. For brevity, only eight fragments derived from eight representative cellular amino acids were shown in the table. The total experimental data comprised 16 fragments from 10 cellular amino acids. Results represent the average of three measurements. Considering the standard deviation in the range from 0.002 to 0.006 for mass distribution, only mass signals of *m*, *m+1*, and *m+2* were compared.

which were responsible for the GCD pathway, were measured in the pellet fraction as well as in the supernatant fraction of the cell extracts. It was found that no GCD activity could be detected in both fractions, indicating that GCD pathway is inactive in the mutant.

Although much valuable information on metabolic response to *gnd* deletion could be obtained from the enzyme activity analysis, the quantitative analysis of this metabolic consequence cannot usually be inferred from in vitro enzyme activities, since not all in vivo effector concentrations are clearly known. In spite of this limitation, the enzyme activities offer the important information in identifying the induced reactions for mathematical modeling in the metabolic flux calculation.

3.3. Metabolic flux response to 6PGDH deletion

Here the ^{13}C tracer technique was used to obtain the detailed quantitative discrimination between the mutant and its parent strain. While exponential growth parameters and enzyme activities were obtained in batch cultures, metabolic flux distribution was analyzed in chemostat cultures for the sake of isotopomer balance under the well-defined steady state as required by the mathematical modeling [9,10]. Despite this difference in culture condition, since a physiological steady state could also be attained during the exponential growth phase in batch cultures [2], the metabolic flux analysis obtained from continuous cultures is expected to be able to interpret the cellular re-

Table 4
Measured and simulated values of the 2D HMQC NMR spectra of cellular amino acids

Atom	Wild-type								*gnd* mutant							
	measured				simulated				measured				simulated			
	s	d_1	d_2	*dd*	*s*	d_1	d_2	*dd*	*s*	d_1	d_2	*dd*	*s*	d_1	d_2	*dd*
Ala: α	0.10	0.03	0.11	0.76	0.03	0.00	0.17	0.80	0.06	0.02	0.10	0.82	0.01	0.00	0.05	0.93
Ala: β	0.28	0.72	~	~	0.30	0.70	~	~	0.34	0.66	~	~	0.32	0.68	~	~
Arg: δ	0.81	0.19	~	~	0.87	0.13	~	~	0.92	0.08	~	~	0.88	0.12	~	~
Leu: δ1	0.38	0.62	~	~	0.30	0.70	~	~	0.27	0.73	~	~	0.32	0.68	~	~
Leu: δ2	0.83	0.17	~	~	0.90	0.10	~	~	0.86	0.14	~	~	0.91	0.09	~	~
His: β	0.06	0.09	0.05	0.80	0.01	0.05	0.00	0.94	0.05	0.22	0.03	0.70	0.00	0.17	0.00	0.83
Ser: β	0.35	0.65	~	~	0.31	0.69	~	~	0.29	0.71	~	~	0.32	0.68	~	~
Thr: γ	0.92	0.08	~	~	0.87	0.13	~	~	0.80	0.20	~	~	0.88	0.12	~	~
Asp: α	0.12	0.05	0.39	0.44	0.09	0.01	0.42	0.48	0.18	0.09	0.41	0.32	0.13	0.02	0.52	0.33
Gly: α	0.12	0.88	~	~	0.07	0.93	~	~	0.10	0.90	~	~	0.01	0.99	~	~

The simulated values are from the estimated flux distribution given in Figs. 1 and 2.

sponse as shown in the physiological and enzymatic analysis.

The modified minimization algorithm was used to estimate net fluxes and exchange coefficients on the basis of the experimental data. Totally 16 fragments from 10 cellular amino acids and 26 multiplet patterns from 10 carbons of 8 cellular amino acids were used for GC-MS and NMR spectra analysis. The deviation between experimental and predicted data is shown in Tables 3 and 4. For brevity, only eight fragments from eight representative cellular amino acids are shown in the Table 3 with others omitted. In the case of all the data, there was no set of measurements with particularly large deviation between the predicted and the measured signals, proving that the mathematical modeling which rigorously considered the excessive information obtained with tracer experiments was reliable for characterizing the metabolic fluxes in vivo. There are two reasons for the relatively large differ-

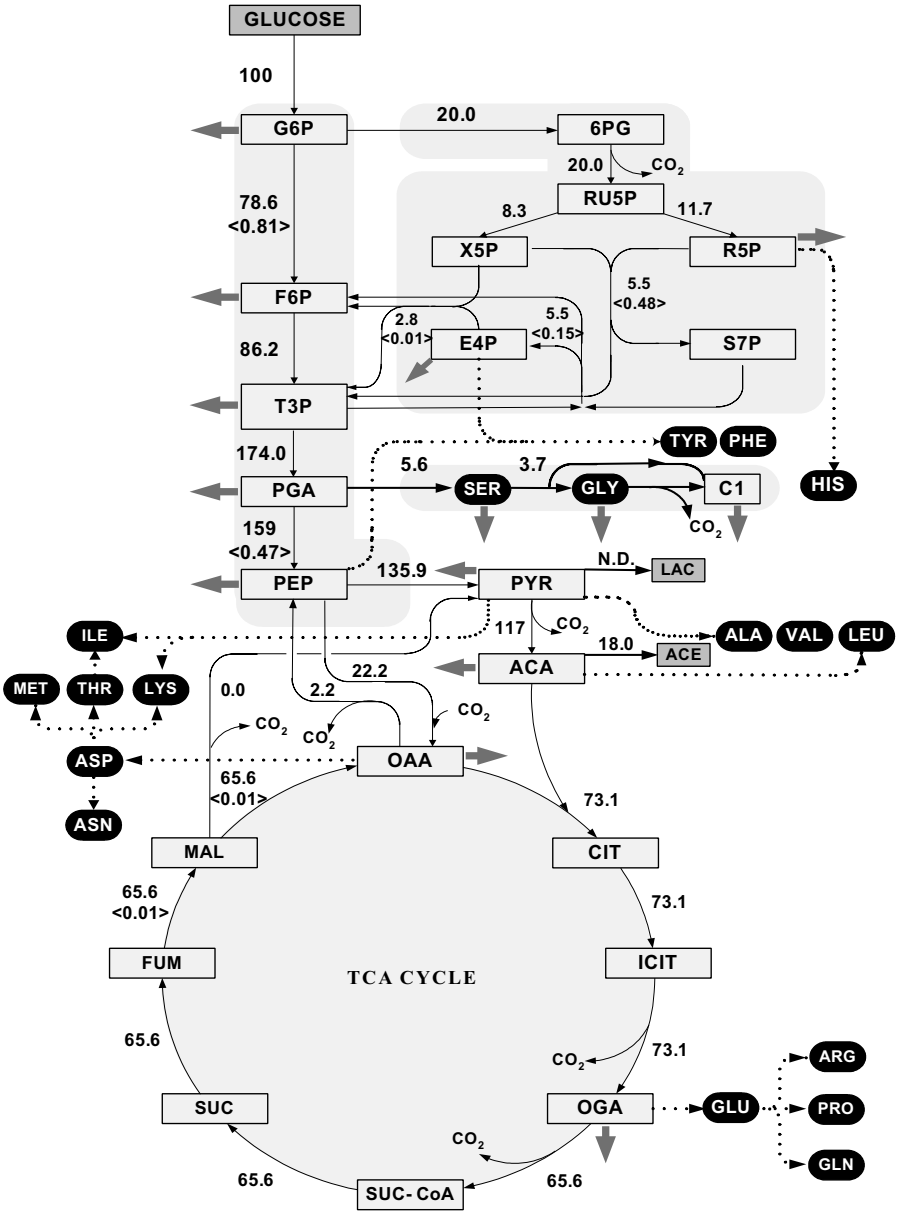

Fig. 1. Metabolic flux distribution in chemostat culture of *E. coli* BW25113 at a dilution rate of 0.2 h^{-1}. Fluxes are given relative to the specific glucose consumption rate (3.20 mmol g^{-1} h^{-1}) and are expressed as the net fluxes for the central metabolism. Arrowheads indicate the primary direction of fluxes in a given reaction. Dashed lines indicate the relationships of cellular amino acids to their precursors. Shaded arrows indicate the withdrawal of precursors for biosynthesis. The exchange coefficients are shown in brackets for the reactions that were considered reversible. Amino acids are indicated by their three-letter code. Abbreviations: ACA, acetyl coenzyme A; CIT, citrate; E4P, erythrose-4-phosphate; F6P, fructose-6-phosphate; FUM, fumarate; G6P, glucose-6-phosphate; ICIT, isocitrate; MAL, malate; LAC, lactate; OAA, oxaloacetate; OGA, oxoglutarate; PYR, pyruvate; PEP, phosphoenolpyruvate; PGA, 3-phosphoglycerate; R5P, ribose-5-phosphate; RU5P, ribulose-5-phosphate; S7P, sedoheptulose-7-phosphate; SUC, succinate; SUC-CoA, succinylcoenzyme-A; T3P, glyceraldehydes-3-phosphate; X5P, xylulose-5-phosphate; 6PG, 6-phosphogluconate; KDPG, 2-keto-3-deoxy 6PG; ACE, acetate; N.D., could not be detected by instrument analysis.

ence between measured and simulated values of the β carbon of His in 2D HMQC NMR. The one attributed to the low concentration of His after HCl hydrolysis of the biomass protein, which reduced the signal-to-noise of NMR acquisition characterized by relatively low sensitivity. The other ascribed to the interference of long-range ^{13}C–^{13}C scalar coupling on the measured one-bond ^{13}C–^{13}C scalar coupling [20].

The best-fit flux distribution of two strains is given in Figs. 1 and 2. Obviously, several noteworthy characteristics have been found by this quantitative description of the flux distribution. In the case of the PPP, the *gnd* deficiency elicited three important differences between two strains. First, the wild-type directed 20% of total carbon flux through the glucose-6-phosphate dehydrogenase, but the relative flux was decreased to the half in the mutant. This reduction corroborates the tendency observed in the analysis of *P. isomerase* and glucose-6-phosphate dehydrogenase specific activities (see Table 2). Second, the block of the 6PGDH pathway had consequence on the direction of the fluxes involved in the non-oxidative pathway. The highly reversible reactions catalyzed by transaldolase I, II and transaldolase were found in a direction opposite to those of the wild-type. Third, evidence for the presence

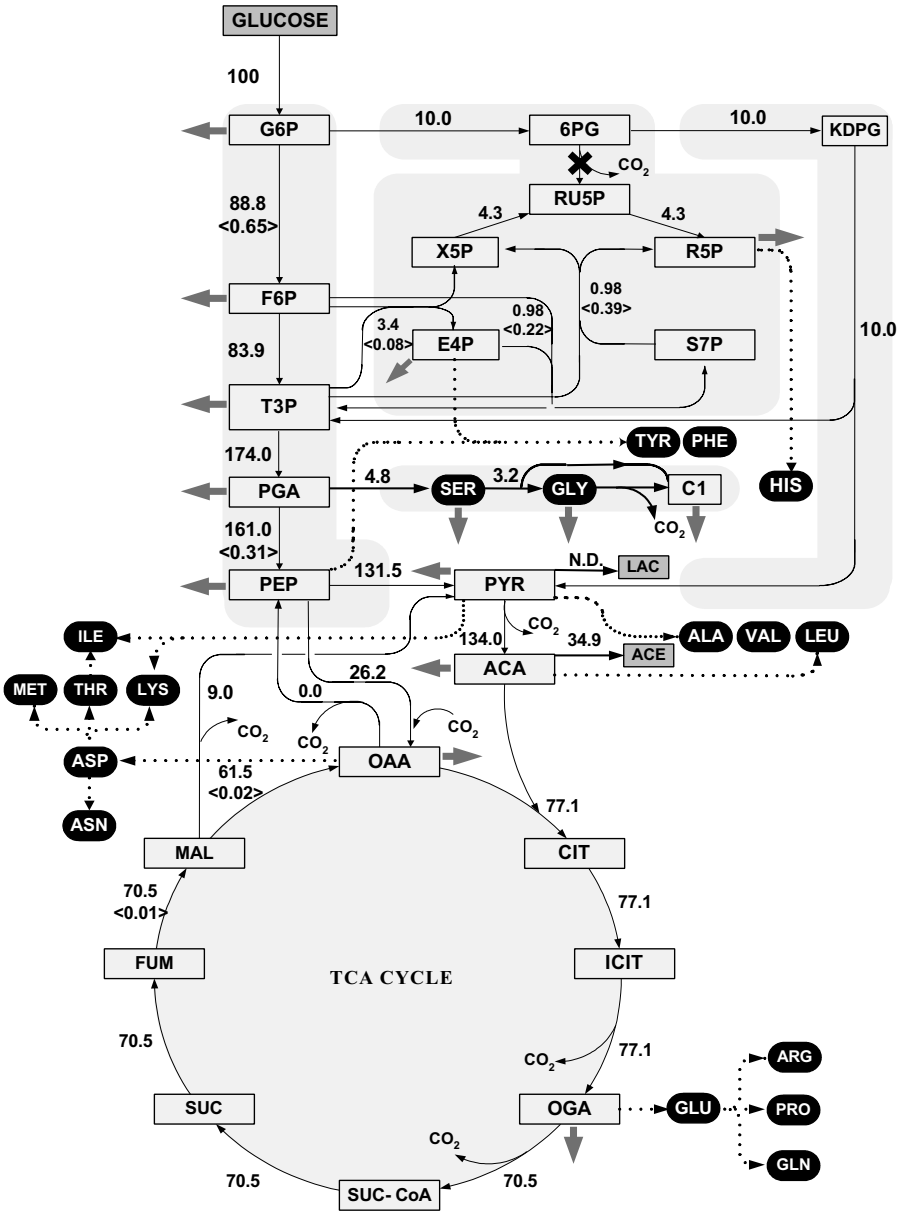

Fig. 2. Metabolic flux distribution in chemostat culture of *gnd* knock-out mutant at a dilution rate of 0.2 h^{-1}. Fluxes are given relative to the specific glucose consumption rate (3.75 mmol g^{-1} h^{-1}) and are expressed as the net fluxes for the central metabolism. For figure description and abbreviations, see the legend to Fig. 1.

of the enzymes of the ED-pathway was confirmed by the metabolic flux analysis. These differences are attributed to the function of PPP in the central metabolism. Since oxidative PPP is the main source for ribose and NADPH formation during the cellular metabolism, the blockage in 6PGDH reaction induced a compensatory mechanism within PPP to compensate for this disturbance. The existence of the ED-pathway could reduce the 6-phosphogluconate accumulation, thus keeping the glucose-6-phosphate dehydrogenase still active so as to produce NADPH for biosynthetic reactions. Normal cells produce ribose mainly via oxidative PPP, while the mutant utilized intermediates of EMP to synthesize ribose and E4P. In biochemistry, this pattern of ribose formation only took place when most of glucose-6-phosphate is converted to fructose-6-phosphate and glyceraldehyde-3-phosphate. This is strongly supported by the mutant with increased flux entering EMP.

In addition to the flux rerouting and direction reversing within PPP, another compensatory mechanism with respect to anaplerotic metabolism was induced by the *gnd* deletion. The inactivation of 6PGDH and the accompanied decrease in the flux through glucose-6-phosphate dehydrogenase reduced the NADPH reaction. As we know, these two reactions are the main sources for NADPH supply inside the normal cells. Therefore, other NADPH-producing reactions were expected to be active so as to complement the reducing power used for the cell growth. In the *gnd* knock-out *mutant*, this supplement was manifested in the activation of *malic enzyme*, by which NADPH was produced using malate, an intermediate of the TCA cycle. This drain of carbon skeletons from the TCA cycle enabled the cells to respond to TCA carbon depletion by regulating the carbon flux through *ppc* and *pckA*. This regulation was to respond to the depletion of OAA in the TCA cycle resulting from the increase of the carbon flux by way of *malic enzyme*. To increase the net synthesis of OAA from phosphoenolpyruvate, *ppc* was therefore up-regulated and *pckA* was down-regulated in the mutant.

When considering all the fluxes that contributed to CO_2 production and consumption, the CO_2 evolution rate relative to the specific glucose consumption rate for the wild-type and the mutant was 2.56 and 2.64, respectively, confirming that there is only minor difference in respiratory metabolism between the mutant and its parent strain.

Acknowledgements

It is acknowledged that the research was supported in part by a grant from New Energy and Industrial Technology Development Organization (NEDO) of the Ministry of Economy, Trade and Industry of Japan (Development of a Technological Infrastructure for Industrial Bioprocess Project).

References

[1] Emmerling, M., Dauner, M., Ponti, A., Fiaux, J., Hochuli, M., Syzperski, T., Wuthrich, K., Bailey, J.E. and Sauer, U. (2002) Metabolic flux responses to pyruvate kinase knockout in *Escherichia coli*. J. Bacteriol. 184, 152–164.

[2] Canonaco, F., Hess, T.A., Heri, S., Wang, T., Szyperski, T. and Sauer, U. (2001) Metabolic flux response to phosphoglucose isomerase knock-out in *Escherichia coli* and impact of overexpression of the soluble transhydrogenase UdhA. FEMS Microbiol. Lett. 204, 247–252.

[3] Fraenkel, D.G. (1968) Selection of mutants lacking glucose-6-phosphate dehydrogenase or gluconate-6-phosphate dehydrogenase. J. Bacteriol. 95, 1267–1271.

[4] Sprenger, G.A. (1995) Genetics of pentose-phosphate pathway enzymes of *Escherichia coli* K12. Arch. Microbiol. 164, 324–330.

[5] Wittmann, C. and Heinzle, E. (1999) Mass spectrometry for metabolic flux analysis. Biotechnol. Bioeng. 62, 739–750.

[6] Marx, A., Graaf, A.A., Wiechert, W., Eggeling, L. and Sahm, H. (1996) Determination of the fluxes in the central metabolism of Corynebacterium glutamicum by nuclear magnetic resonance spectroscopy combined with metabolite balancing. Biotechnol. Bioeng. 49, 111–129.

[7] Winden, V., Schipper, D., Verheijen, P. and Heijnen, J. (2001) Innovations in generation and analysis of 2D [(13)C, (1)H] COSY NMR spectra for metabolic flux analysis purposes. Metab. Eng. 3, 322–343.

[8] Datsenko, K.A. and Wanner, B.L. (2000) One-step inactivation of chromosomal genes in *Escherichia coli* K12 using PCR products. Proc. Natl. Acad. Sci. USA 97, 6640–6645.

[9] Zhao, J. and Shimizu, K. (2002) Metabolic flux analysis of *Escherichia coli* K12 Grown on ^{13}C-labeled acetate and glucose using GC-MS and powerful flux calculation method. J. Biotechnol., in press.

[10] Dauner, M., Bailey, J.E. and Sauer, U. (2001) Metabolic flux analysis with a comprehensive isotopomer model in *Bacillus subtilis*. Biotechnol. Bioeng. 76, 144–156.

[11] Lowry, O.H., Rosebrough, N.J., Farr, A.L. and Randall, R.J. (1951) Protein measurement with the Folin Phenol reagent. J. Biol. Chem. 193, 265–275.

[12] Sauer, U., Lasko, D.R., Fiaux, J., Hochuli, M., Glaser, R., Szyperski, K.W. and Bailey, J.E. (1999) Metabolic flux ratio analyis of genetic and environmental modulations of *Escherichia coli* central carbon metabolism. J. Bacteriol. 181, 6679–6688.

[13] Colowick, S.P. (1963) Preparation and assay of enzymes. Methods Enzymol. 6, 1–640.

[14] Szyperski, T. (1995) Biosynthetically directed fractional ^{13}C-labeling of proteinogenic amino acids - An efficient analytical tool to investigate intermediary metabolism. Eur. J. Biochem. 232, 433–448.

[15] Paul Lee, W.N. (1991) Mass isotopomer analysis: theoretical and practical consideration. Biol. Mass Spectrometry 20, 451–458.

[16] Schmidt, K., Nielsen, J. and Villadsen, J. (1999) Quantitative analysis of metabolic fluxes in *Escherichia coli* using two-dimensional NMR spectroscopy and complete isotopomer models. J. Biotechnol. 71, 175–190.

[17] Neidhardt, F.C., Ingraham, J.L. and Schaechter, M. (1990) Physiology of the Bacterial Cell: A Molecular Approach. Sinauer Associate, Sunderland Inc., MA.

[18] Schmidt, K., Nielsen, J. and Villadsen, J. (1997) Modeling isotopomer distributions in metabolic networks using isotopomer mapping matrices. Biotechnol. Bioeng. 55, 831–840.

[19] Matsushita, K., Arents, J.C., Bader, R., Yamada, M., Adachi, O. and Postma, P.W. (1997) *Escherichia coli* is unable to produce pyrroloquinoline quinine (PQQ). Microbiology 143, 3149–3156.

[20] Winden, W.V., Schipper, D., Verheijen, P. and Heijnen, J. (2001) Innovations in generation and analysis of 2D [^{13}C, ^{1}H] COSY NMR spectra for metabolic flux analysis purposes. Metab. Eng. 3, 322–343.